Seamless Stitching of Graphene Domains on Polished Copper (111) Foil

*Van Luan Nguyen, Bong Gyu Shin, Dinh Loc Duong, Sung Tae Kim, David Perello, Young Jin Lim, Qing Hong Yuan, Feng Ding, Hu Young Jeong, Hyeon Suk Shin, Seung Mi Lee, Sang Hoon Chae, Quoc An Vu, Seung Hee Lee, and Young Hee Lee**

Graphene grain boundaries (GGBs) are inevitably formed via stitching of graphene flakes, consequently limiting the graphene quality.[1,2] There have been numerous reports that GGBs are a primary carrier scattering source, thus degrading the related device performance.[2–8] Therefore, it is always desired to obtain large-area graphene without forming GGBs. Two approaches exist for synthesizing monocrystalline graphene. One approach is to reduce the number of nucleation seeds, for example, using annealed copper foil at high temperature,[9,10] preoxidized copper,[11–13] or polished copper foil.[1,2] However, large-area growth is terminated by an unknown self-limiting growth factor and requires long growth time. Another approach entails the alignment of graphene domains while leading them to stitch together to form uniform single monocrystalline graphene. Thus, seamless stitching of graphene domains during chemical vapor deposition (CVD) is an ideal concept to realize large-area monocrystalline graphene. Although hydrogen-terminated Ge(110)[14] overlayer on Si substrate adopts weakly interacting graphene monolayer to realize this concept, formation of simple defects or impurities on Ge(110) surface particularly in large area could easily break this condition, making it difficult to synthesize graphene with high uniformity and reproducibility. In contrast, Cu(111) substrate maintains hexagonal symmetry with minimum lattice mismatch with graphene and attempts have been made to try to grow graphene, but no evidence for seamless stitching has been provided.[15–19] The question is further obscured by introducing graphene growth on Ni substrate,[20] where a grain boundary exists between two graphene domains in the same orientation, in contrast with the graphene growth on Ge[14] and h-BN[21] substrates. Use of copper substrate is technologically relevant, since monolayer graphene is easily tailored due to the limited carbon solubility in copper, and moreover the surface morphology can be controlled at large area with low cost.

In this paper, we prove the concept of seamless stitching without forming GGBs by preparing Cu(111) foil for CVD. Cu foil was further polished by chemical–mechanical polishing (CMP) method followed by annealing at 1075 °C. This process was repeated several times until Cu(111) orientation was achieved. The hexagonal shape of the graphene domains was achieved by maintaining a high ratio of H_2/CH_4 of 1600, i.e., a slow carbon feedstock where carbon atoms can reach energetically favorable sites. The seamless stitching was realized by merging hexagonal graphene domains in the same orientation on polished Cu(111) surface and verified by not only atomic-scale images by scanning tunneling microscopy (STM) and transmission electron microscopy (TEM) at the corner that was formed by two edges of merged domains, but also by macroscale images from optical microscopy after UV-treatment at the stitched region of the merged domains.[2] This was markedly distinct from the clear GGBs formed by the similar hexagonal domains

V. L. Nguyen, Dr. B. G. Shin, Dr. D. L. Duong, S. T. Kim, Dr. D. Perello, Dr. S. H. Chae, Q. A. Vu, Prof. Y. H. Lee
IBS Center for Integrated Nanostructure Physics
Institute for Basic Science (IBS)
Sungkyunkwan University
Suwon 440-746, Republic of Korea
E-mail: leeyoung@skku.edu

V. L. Nguyen, S. T. Kim, Q. A. Vu, Prof. Y. H. Lee
Department of Energy Science
Department of Physics
Sungkyunkwan University
Suwon 440-746, Republic of Korea

Dr. Y. J. Lim, Prof. S. H. Lee
Department of BIN Fusion Technology and Department of Polymer-Nano Science and Technology
Chonbuk National University
Jeonju, Jeonbuk 561-756, Republic of Korea

Dr. Q. H. Yuan
Department of Physics
East China Normal University, No. 500
Dongchuan Road, Shanghai, China

Prof. F. Ding
Institute of Textiles and Clothing
The Hong Kong Polytechnic University
Kowloon, Hong Kong SAR

Prof. H. Y. Jeong
Central Research Facilities
Ulsan National Institute of Science and Technology (UNIST)
Ulsan 689-798, Republic of Korea

Prof. H. S. Shin
Interdisciplinary School of Green Energy
Low Dimensional Carbon Materials Center and School of Mechanical and Advanced Materials Engineering
Ulsan National Institute of Science and Technology (UNIST)
Banyeon-ri 100, Ulsan 689-805, Republic of Korea

Dr. S. M. Lee
Center for Nanomaterials Characterization
Korea Research Institute of Standards and Science
Daejeon 305-340, Republic of Korea

DOI: 10.1002/adma.201404541

© 2014 WILEY-VCH Verlag GmbH & Co. KGaA, Weinheim

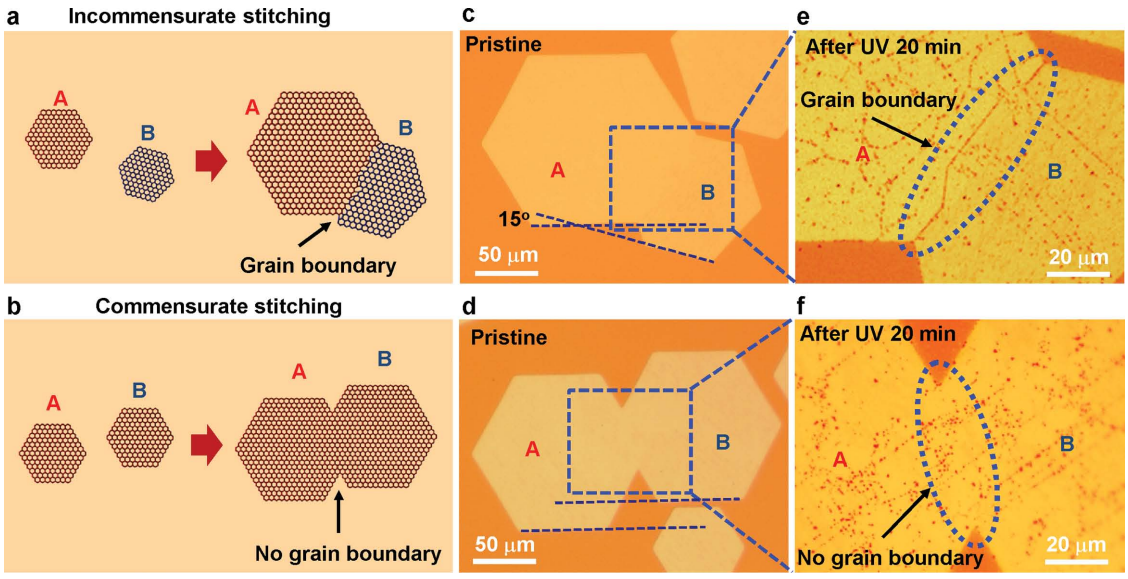

Figure 1. Incommensurate and commensurate stitching of two hexagonal graphene domains: a, b) Schematic of incommensurate and commensurate stitching of two hexagonal graphene domains in different and in same orientations. c,d) Respective images of optical microscopy from pristine samples. e,f) UV-light irradiated samples under 50% moisture conditions for 20 min. A clear graphene boundary line was observed for incommensurate stitching, while no such boundary line was observed for commensurate stitching.

in different orientations, in congruent with our density–functional calculations. This concept was extended to synthesize monocrystalline graphene of 6 cm × 3 cm size by CVD for an hour by merging multiple hexagonal graphene domains in the same orientation on polished Cu(111) foil. The monocrystalinity of the large-area sample was confirmed by a new observation method achieved by correlating confocal Raman mapping on overlapped graphene bilayers to polarized optical microscopy (POM) on spin-cast nematic liquid crystal (NLC) layer, combined with transport measurements at the stitched region.

Figure 1 shows examples of incommensurate stitching between two hexagonal graphene domains with GGBs and commensurate stitching without GGBs. A simple optical microscopy image could not identify the GGB line (Figure 1c, d). By using UV exposure under moisture ambient conditions, which was described clearly in our previous report,[2] a clear GGB line was observed in incommensurate stitching, where the edge directions of two hexagonal graphene domains were mismatched by 15° (Figure 1c,e). Conversely, no GGB line was observed after identical UV exposure in commensurate stitching, where the edge directions of two hexagonal graphene domains were identical (Figure 1d,f; see more examples in Figure S1 and S2, Supporting Information). A similar phenomenon was also observed by conductive atomic-force microscopy (AFM) mapping (Figure S3, Supporting Information).

Identification of lattice orientation in each domain is important to understand the stitching. **Figure 2**a,b demonstrates an example of two lattice orientations within a nearly hexagonal domain, which can presumably be regarded as a monocrystalline domain.[9,12] UV exposure reveals a clear GGB as triangular (Figure 2b). The NLC droplet was spin-cast onto this graphene on copper directly. By using the reflection mode of POM (see Experimental Section), a clear triangular flake, merged within the hexagonal domain, was then observed (Figure 2c) similar to what is shown in Figure 2b. Angle-dependent POM images revealed a different contrast due to a different orientation of the liquid crystal (LC) director, while no distinctive difference was observed without a polarizer and, therefore, this domain could be regarded mistakenly as a monocrystalline graphene (Figure S4, Supporting Information). This implies that the director of LC molecules is aligned to a preferred direction of graphene lattice within the domain. This was further confirmed by density functional calculations. AB stacking between hexagons in graphene and hexagonal rings in LC molecules is energetically more favorable (Figure S5, Supporting Information). In order to use the transmission mode of POM (see Experimental Section), graphene domains were transferred onto a glass substrate, and by using an analyzer and a polarizer, the absolute lattice orientation of graphene domains can in fact be featured (Figure S6, Supporting Information). Two hexagonal domains were stitched together with orientations of 90° and 135°. More importantly, we found that the orientation mismatch of the LC molecules is the same as the edge mismatch of the two graphene domains. This paper is contrasted with a previous report in which a similar NLC droplet method was used to identify the graphene lattice orientation but was misled by the Cu grain orientation.[22]

Orientation mismatch was further confirmed by overlapping another monocrystalline graphene domain (see Experimental Section), as shown by the contrast difference under an optical microscope (Figure 2d and Figure S7, Supporting Information). Three distinct regions of contrast near the triangular flake are shown in the confocal Raman mapping of the 2D band (Figure 2e,f). Region 1 shows top monolayer graphene with a small 2D intensity. The intensity of the 2D band was increased in region 2 due to weak interaction between the two-folded layers,[23–25] which is a clear indication of a large misorientation angle. In contrast, the 2D intensity in region 3 was significantly

© 2014 WILEY-VCH Verlag GmbH & Co. KGaA, Weinheim

ADVANCED MATERIALS
www.advmat.de

www.MaterialsViews.com

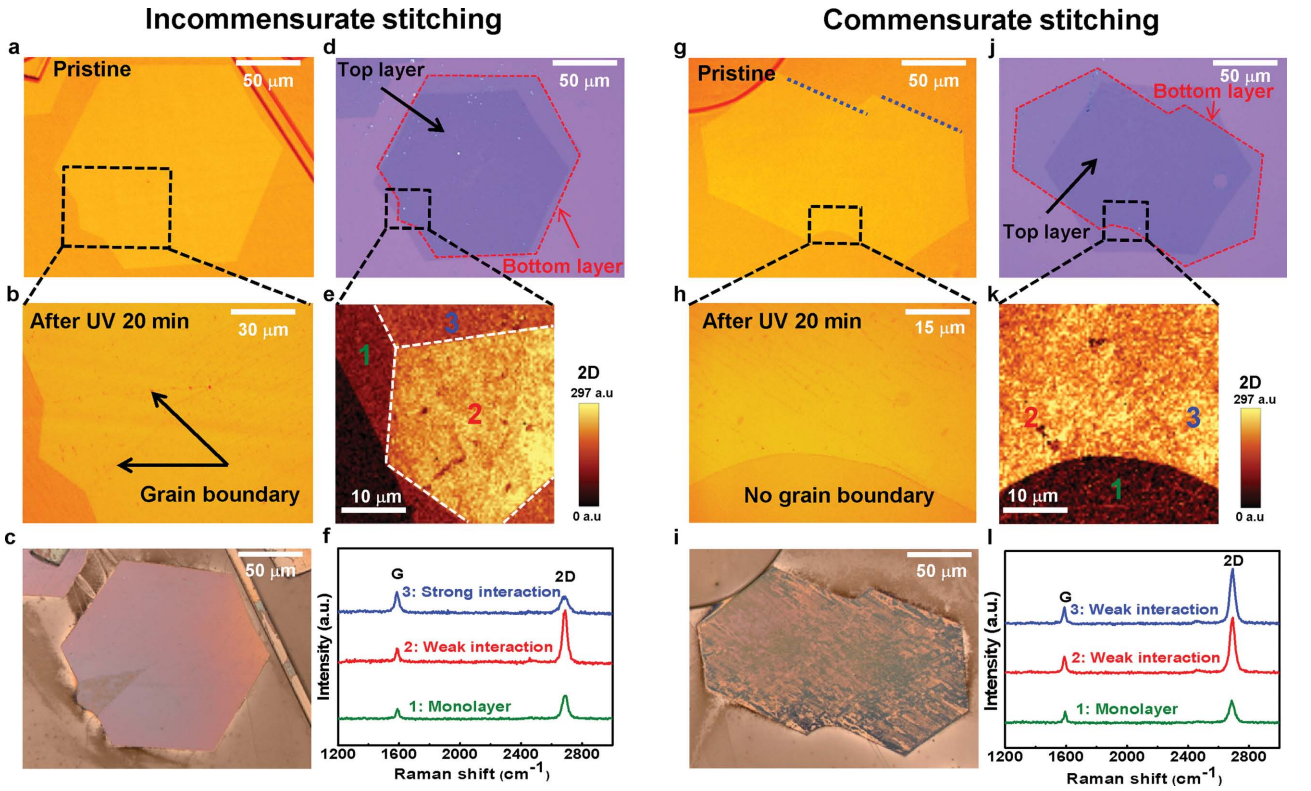

Figure 2. Observation of GGB and grain orientation with LC and Raman spectroscopy: a–f) Incommensurate stitching. Optical microscopy images of a) two pristine graphene domains merged within hexagon (GGB line is invisible) and b) UV-irradiated sample (GGB line is visible). c) POM image (triangular internal flake became noticeable using reflected mode). Dark (bright) means LC director to be perpendicular (parallel) to the polarizer. d) Optical image of two graphene layers by overlapping another single crystalline monolayer graphene. e,f) Confocal Raman mapping of 2D band in the triangular region and the corresponding Raman spectra. g–l) Similar demonstration for commensurate stitching. No GGB line was observed in (h). No contrast difference in POM image (i) nor in 2D band mapping between region 2 and 3 (k,l).

reduced, indicating strong interaction between the two layers. This observation of different orientations of two overlapped graphene layers is well corroborated with Figure 2c.

Figure 2g shows another example of commensurate stitching. UV exposure did not reveal a GGB line (Figure 2h and Figure S2, Supporting Information) and the orientation of the two graphene domains was identical (Figure 2i). Although a different contrast was observed by rotating polarizer direction, no clear distinction between the two domains was visible (Figure S8, Supporting Information). After another monocrystalline graphene was overlapped (Figure 2j), similar to what is shown in Figure 2d, no difference in 2D intensity mapping was observed between the two domains (Figure 2k). Raman spectra in region 2 and region 3 were also similar (Figure 2l). Full Raman mapping of the G band intensity and 2D/G intensity ratio, with more samples for both incommensurate and commensurate stitching were shown in Figures S9 and S10, Supporting Information. It is of note that a round shape edge was formed (Figure 2h) at a 120° corner, whereas at a 60° corner, the merged corner still remained sharp (Figure S11, Supporting Information). This is ascribed to more arriving carbon atoms at 120° corner due to larger available Cu area.

Our optical microscopy and confocal Raman spectroscopy provided evidence of no grain boundaries in commensurate stitching at the macroscale. Here we provide evidence of seamless stitching at atomic scale by STM measurements (see Experimental Section). This was realized by focusing the corner of two merged hexagonal graphene domains on copper without transfer. This approach is advantageous compared to TEM observations involving transfer process which often leads to formation of wrinkles and residues. **Figure 3**a shows optical image of the merged graphene domains marked by the green dashed lines for commensurate case, red dashed line indicates hypothetical grain boundary (Figure S12, Supporting Information). STM image near the corner (Figure 3b) shows graphene on the stepped copper surface. The enlarged STM image across the hypothetical grain boundary (Figure 3c) shows complicated morphology of graphene on copper surface with Moiré patterns, which consisted of steps (wide bright stripes) and terraces (narrow dark grooves). Regular corrugation shown in region 1 in the inset with a period of 0.6 nm comes from copper steps, congruent with previous report.[26] Thus, any grain-boundary feature around 1 nm should be visible in this scale if it exists.[27,28] No clear evidence for the existence of grain boundary was noticed. Different feedback current shows clearly honeycomb graphene structure (1*). Enlarged STM images in two different regions across the hypothetical line (2 and 3) show the identical orientation (Figure 3d). One dimensional regular Moiré pattern with honeycomb graphene in the inset at high resolution was clearly observed (H). The insets in Figure 3d

© 2014 WILEY-VCH Verlag GmbH & Co. KGaA, Weinheim

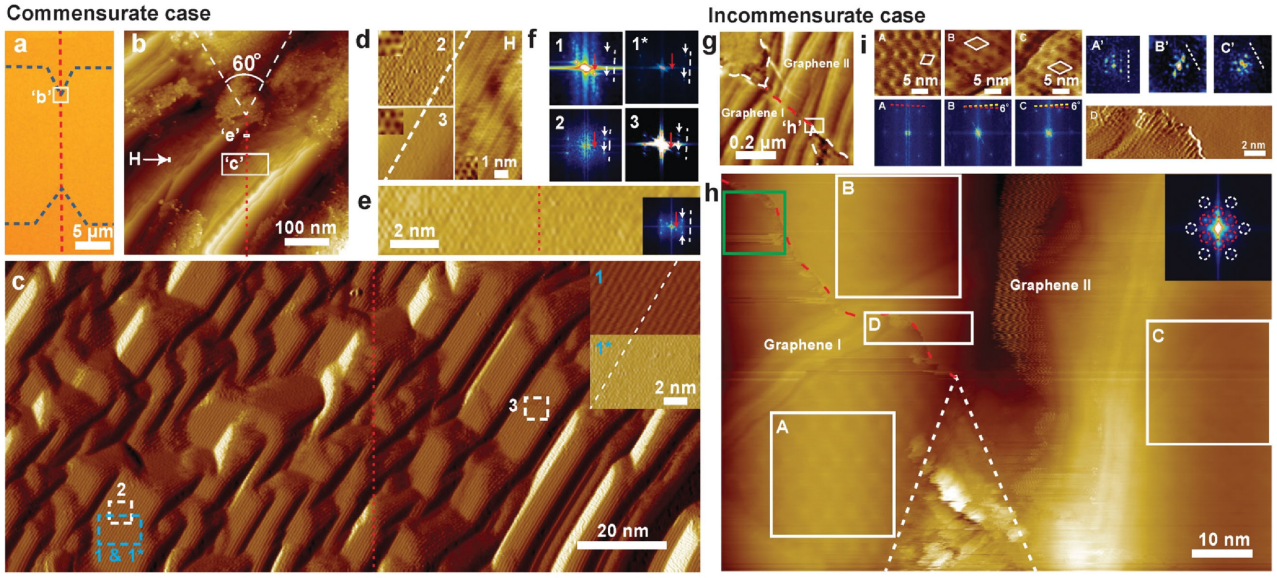

Figure 3. STM observations at the merged region in commensurate and incommensurate stitching of graphene. Commensurate case: a) Optical image of stitching area. The green dashed and red dashed lines indicate respective graphene region and hypothetical grain boundary. b) STM image (constant current mode) of the region near the corner marked in (a). c) STM image (constant height mode) marked in b) consisting of steps (wide bright stripes) and terraces (narrow dark grooves) across hypothetical boundary. Inset: 1 and 1*: low- and high-feedback current level, indicating clear stepped surface and honeycomb graphene structure, respectively. d) Enlarged STM images of (b,c). 2 and 3 located on the left and right domains have the same orientation to each other. Another point (H) on the left domain shows the identical orientation. Moiré pattern is visible. Insets show honeycomb graphene at atomic scale. e) Enlarged image of (b) across the hypothetical boundary. No misfit graphene boundary was observed and confirmed by FFT of the region. f) The FFT results of each region. Red and white arrows indicate respective Moiré and graphene peaks. All indicate the identical orientation. Incommensurate case: g) STM image (constant current mode) locating the stitched area indicated by the long-dashed lines. h) Enlarged STM image near the corner of (g). Grain boundary line is visible (red line). Inset shows boundary scattering (red circles) inside graphene peaks (white circles). i) Enlarged STM images of (h) and the corresponding FFTs results. (B,C) are in the same domain, identified by FFTs but deviated from (A) by 6°. Steps in (B,C) do not contribute to FFT peaks. A', B', C': FFTs of enlarged Moiré patterns. D: Enlarged grain boundary.

also indicate clear honeycomb graphene structure. Atomic resolution image of the "e" position in Figure 3b revealed neither grain boundaries nor poor fitting of two domains (Figure 3e). The corresponding FFT results identified the same graphene orientation in different domains (white arrows or lines) (see Figure S13, Supporting Information for detailed analysis), the peaks related to the corrugation lines were also visible by red arrows (Figure 3f). Similar phenomena in other positions at the corner were also observed (see Figure S13, Supporting Information). Our STM observations at atomic scale and nanoscale well match with macroscale observation of optical microscopy (Figure 1f, Figure 2h) and confocal Raman mapping (Figure 2k), and clearly prove the seamless stitching in commensurate case. The lattice mismatch between copper (111) and graphene is 4%.[29] The two adjacent graphene domains may not match atomically, even though they have the same orientation. More importantly, graphene was synthesized at high temperature, weak coupling with copper (111) causing low friction of graphene on copper. At this temperature, the Cu surface is nearly a liquid state, while graphene domains remain crystallized. When graphene domains merge together, still do care about energy minimization at the stitched area to form commensurate stitching but the substrate effect is ignored due to liquid state. During cooling, the strain energy on graphene due to the lattice mismatch cannot strongly influence the already formed graphene lattice. This kinematical behavior requires further detailed study.

In contrast, a grain boundary at the corner (marked by the red dashed line) appears in incommensurate case (Figure 3g). The enlarged STM image of the corner in Figure 3g is shown in Figure 3h, the evidence of grain boundary was indicated more clearly. Remarkably, in the same scan range, there is no such evidence of grain boundary in Figure 3c. The green box includes the grain boundary, where the corresponding FFT results in the inset show honeycomb graphene peaks (white circles) and grain boundary scatterings near the center (red circles). Enlarged STM images of three regions in different domains are listed in Figure 3i. "A" shows a Moiré pattern in flat area with a clear honeycomb graphene at high resolution (inset) (see Figure S14, Supporting Information). "B" and "C" contain step and a Moiré pattern. These steps should be distinguished from grain boundaries since the corresponding FFT results did not show scattering peaks. The misorientation angle of 6° is identified by the graphene peaks in FFTs. The related Moiré patterns (A," B," C") were also shown, again demonstrating different orientations of domains. We emphasize that regions B and C have the identical orientation in the same domain. The enlarged STM image of the grain boundary in D shows complex structures, which requires further study. The observed grain boundary in incommensurate case here is clearly distinct from that in commensurate case.

Commensurate stitching was further confirmed by TEM observations (see Experiment Methods in the Supporting Information). Electron diffraction patterns at the corner with

© 2014 WILEY-VCH Verlag GmbH & Co. KGaA, Weinheim

ADVANCED MATERIALS
www.advmat.de

www.MaterialsViews.com

an angle of 60° at different positions revealed the same orientation, regardless of the position in two different domains (Figure S15, Supporting Information). In order to prove seamless stitching, 60 continuous high resolution TEM images (follow yellow dashed line) were obtained by scanning across the hypothetical grain boundary (red dashed line). No evidence of grain boundary was observed except the folded line due to wrinkles. However, possibility of grain boundary line to overlap with the folded lines is very unlikely, since those wrinkles are far from the hypothetical line (see Figure S16, Supporting Information). These again revealed the seamless stitching.

The seamless stitching was confirmed by measuring sheet resistance across the boundary with Hall-bar structures (Figures S17 and S18, Supporting Information). No appreciable maximum resistance change or Dirac point shift was observed in commensurate case (Figure S19a, c, Supporting Information). This implies that no additional sheet resistance exists at the stitched region and the two domains are electrically homogeneous. In other words, the boundary in commensurate stitching is electrically transparent. In contrast, in incommensurate stitching, the maximum sheet resistance increased by ≈60% near the boundary (4–5 pairs), while all other values remained nearly the same. Dirac points varied from position to position, indicating inhomogeneity of the two domains (Figure S19b,d, Supporting Information). The average field effect mobility over the whole device for 0–9 electrode was 6100 (5700) $cm^2\ V^{-1}s^{-1}$ for electrons (holes) in commensurate stitching, larger than 3200 (2900) $cm^2\ V^{-1}\ s^{-1}$ for electron (hole) in incommensurate stitching. The lower mobility in incommensurate stitching may originate from the presence of wrinkles on copper foil (Figure S21, Supporting Information).

To investigate how to control alignment of graphene domains that may lead to all commensurate stitching, we further studied copper orientation dependence. **Figure 4**a shows graphene domains grown on polished polycrystalline Cu foil and the related electron backscattering diffraction (EBSD) image. Although a large area of Cu(111) surface is mainly shown, several other surfaces in general coexist. The general trend is that the orientation mismatch angle between graphene domains is almost zero in polished Cu(111) surfaces and large in other surfaces (Figures S22–S25, Supporting Information). The occurrence of zero misorientation angle was nearly 98%

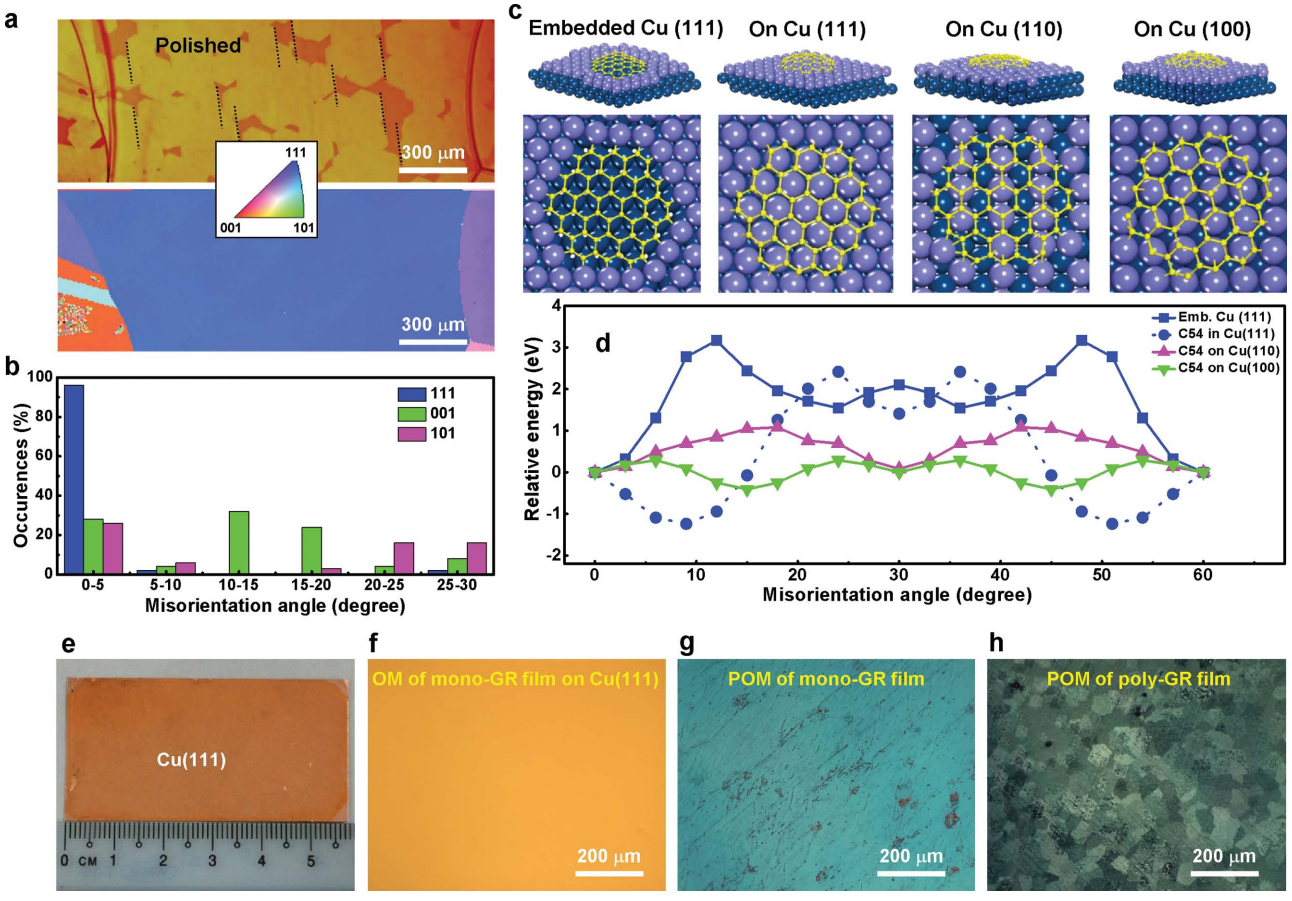

Figure 4. Large-area monocrystalline graphene on Cu(111) substrate: a) Optical image of the graphene grown on polycrystalline Cu foil and the related EBSD mapping of Cu domain orientation. The dotted lines in the top panel indicate orientation of each graphene domain. b) Statistical distribution of misorientation angle of graphene domains in different Cu surfaces. Cu(111) surface can exclusively provide nearly 98% domains of same orientation. c) Various Cu surfaces with a C_{54} cluster: From left, embedded Cu(111), on Cu(111), on Cu(110), and on Cu(100) surfaces. d) Density functional calculations of total energy difference as a function of orientation angle on various Cu substrates. e) Photograph of monocrystalline Cu(111) (6 cm × 3 cm) and f) The related images from optical microscope of complete graphene on copper. Images from POM of complete graphene g) on large-size Cu(111) surface and h) on other surfaces.

© 2014 WILEY-VCH Verlag GmbH & Co. KGaA, Weinheim

on a polished Cu(111) surface (Figure 4b). The remaining 2% at 5–10° is presumably due to impurities or artifacts that may exist on Cu(111) surfaces. This small portion of imperfect alignment can be eliminated using high-purity copper.[16] No GGBs were visible on Cu(111) after UV exposure and many graphene grain boundary lines were observed on Cu(101) and Cu(001) (Figure S26, Supporting Information). Graphene domain mismatch angle was widely distributed from 0° to 30° on other surfaces (Figure 4b and Figure S27, Supporting Information). It is also important to keep the surface clean and flat so as to maintain a zero misorientation angle even for a Cu(111) surface, since the graphene domains were not well-aligned to each other even on unpolished Cu(111) surfaces (Figure S22c, d and S28, Supporting Information). This may explain the previous observation of different orientations of the graphene domains on the same Cu(111) surface.[17,18]

To understand this orientation dependence on Cu surfaces, we performed density functional calculations (Figure 4c,d and Experimental Methods in Supporting Information). Here we adopt a specific graphene growth model on a Cu(111) surface (Figure 4c). The graphene domain (C_{54}) tends to be embedded into a basin of the Cu lattice to realize the distinct growth behavior.[30] Graphene embedded into a Cu(111) surface is strongly confined to the orientation at $\theta = 0°$ (Figure 4d). Once this cluster is anchored, rotation into another orientation is unlikely to happen due to a high rotation barrier height (≈3 eV). This is similar to the step growth observed at relatively high temperature. In the case of graphene floating on a Cu(111) surface, the minimum energy is shifted to ≈9°. Since our growth temperature is high and a basin of Cu lattice with steps is to be formed easily, and therefore graphene growth floating on a bare Cu(111) surface is presumed to be unlikely. For graphene grown on Cu(100) and (110) surfaces, the energy minimum appears at 0° and 30°, respectively. Nonetheless, the energy difference with misorientation angle is relatively small, implying that the misorientation angle distribution can be very broad, in good agreements with experimental observations. This leads to incommensurate stitching of graphene domains.

To prove the concept of well-controlled commensurate stitching of aligned hexagonal graphene domains at a large scale, monocrystalline Cu(111) with a size of 6 cm × 3 cm was used to grow graphene (Figure 4e). This copper was polished by CMP followed by annealing as reported above.[1] It is noted that the aligned-hexagonal graphene domains were retained on the whole Cu(111) surface during the entire growth period (Figure S29, Supporting Information), which is critical to realize the commensurate stitching at a large scale. The complete graphene film was obtained in a relatively short growth time of 1 h, which is another advantage compared with a single graphene domain approach (Figure 4f and Figure S30, Supporting Information).[10–12] No particular contrast was observed in the POM image with the LC layer (Figure 4g and Figure S31, Supporting Information), confirming the formation of seamless monocrystalline graphene. This was well distinguished from conventional polycrystalline graphene growth on various Cu surfaces, (Figure 4h), which led to different contrasts in POM (Figure S32, Supporting Information).

In summary, we have observed two types of stitching: i) commensurate stitching, leading to a seamless coalescence of graphene domains on polished Cu(111) surface and ii) incommensurate stitching, leading to formation of grain boundaries in merged graphene, which occurred on Cu surfaces other than (111). The non-existence of grain boundary was proved clearly not only at the atomic scale by STM and TEM observations but also at the macroscale by optical microscopy after UV-treatment. Large-area monocrystalline graphene, which was clearly verified by newly developed confocal Raman observations of overlapped graphene bilayer and polarizing optical microscopy of graphene coated with an LC layer. Using this principle, we were able to obtain 6 cm × 3 cm monocrystalline graphene without grain boundaries on a polished Cu(111) surface, which was limited only by the chamber size. Our approach of commensurate stitching with controlled Cu(111) surface to realize large-area monocrystalline graphene can be utilized for other types of growth of layered materials such as hexagonal BN and transition metal chalcogenides.

Experimental Section

Graphene Growth: A 100-μm-thick copper foil (from Nilaco, 99.96%) was annealed at 1075 °C with 1000 sccm Ar and 500 sccm H_2 for 2 h and was polished using the chemical–mechanical polishing (CMP) method. The polished copper was placed in a 2 in. quartz tube chamber and heated up to 1075 °C with 1000 sccm Ar and 500 sccm H_2 for annealing for 2 h to remove residuals on the copper surface. During the atmospheric CVD growth, the H_2 gas was reduced to 50 and 3 sccm of CH_4 (1% diluted in Ar) or a ratio of H_2/CH_4 of around 1600, was injected. After growth, the CH_4 was turned off and the chamber was cooled to room temperature.

Formation of Overlapped Graphene by Transfer: The bottom test layer of graphene was simply transferred using the poly(methyl methacylate) (PMMA)-supported method. To overlap the second layer on a designated position, we used the mechanical transfer method by controlling the alignment by optical microscopy. Samples were then baked at 100 °C for 1 h.

Scanning Tunneling Microscopy (STM): Scanning tunneling microscopy (STM) was performed in a ultrahigh vacuum (UHV) chamber with a base pressure below 5×10^{-11} Torr at room temperature using a commercial STM (Omicron, UHV LT STM). An STM tip was made of a polycrystalline W wire by electrochemical etching in a 2 M KOH solution and annealed by electron bombardment. CVD-grown graphene on copper was thermally cleaned up to 400 °C by e-beam heating.

Spin-Coating of Nematic Liquid Crystals: Nematic LC (4-Cyano-4′-pentylbiphenyl: 5CB) was purchased from Merck (Germany) (ZLI-4535). The thin LC film was spin-coated on the surface of graphene on copper at 4000 rpm for a minute.

Polarizing Optical Microscopy (POM): Optical microscopy (ZEISS, Axio Imager 2) was used to obtain images of the surface morphologies of the graphene/Cu samples. For the LC experiment in reflection mode, the analyzer was fixed while the polarizer was rotated from 0° to 180°. In the case of the transmittance mode, the graphene was transferred onto glass. The orientation of the LC molecules on the graphene surface was determined by rotating the sample stage (Nikon ECLIPSE E600, Japan) in transmission mode. First, the rotation angle (α) of the sample with retardation of $\lambda/4$ was measured when each domain on the graphene flake was in a dark state. Second, the sample was rotated counter clockwise by 45°. Finally, the $\lambda/4$ film was inserted at 45° with respect to the rotation angle of the sample. At this time, the color of the domain had been changed into white or dark states. The orientations of the LCs in the white and dark state are α and $\alpha + 90°$, respectively.

© 2014 WILEY-VCH Verlag GmbH & Co. KGaA, Weinheim

Supporting Information

Supporting Information is available from the Wiley Online Library or from the author.

Acknowledgements

This work was supported by the Institute for Basic Science (IBS, EM1304) and in part by BK21-Plus through the Ministry of Education, Korea.

Received: October 1, 2014
Revised: November 13, 2014
Published online: December 18, 2014

[1] G. H. Han, F. Güneş, J. J. Bae, E. S. Kim, S. J. Chae, H. J. Shin, J. Y. Choi, D. Pribat, Y. H. Lee, *Nano Lett.* **2011**, *11*, 4144.
[2] D. L. Duong, G. H. Han, S. M. Lee, F. Gunes, E. S. Kim, S. T. Kim, H. T. Kim, Q. H. Ta, K. P. So, S. J. Yoon, S. J. Chae, Y. W. Jo, M. H. Park, S. H. Chae, S. C. Lim, J. Y. Choi, Y. H. Lee, *Nature* **2012**, *490*, 235.
[3] Q. Yu, L. A. Jauregui, W. Wu, R. Colby, J. Tian, Z. Su, H. L. Cao, Z. H. Liu, D. Pandey, D. Wei, T. F. Chung, P. Peng, N. P. Guisinger, E. A. Stach, J. Bao, S. S. Pei, Y. P. Chen, *Nat. Mater.* **2011**, *10*, 443.
[4] A. W. Tsen, L. Brown, M. P. Levendorf, F. Ghahari, P. Y. Huang, R. W. Havener, C. S. Ruiz-Vargas, D. A. Muller, P. Kim, J. Park, *Science* **2011**, *336*, 1143.
[5] O. V. Yazyev, S. G. Louie. *Nat. Mater.* **2010**, *9*, 806.
[6] D. V. Tuan, J. Kotakoski, T. Louvet, F. Ortmann, J. C. Meyer, S. Roche, *Nano Lett.* **2013**, *13*, 1730.
[7] L. A. Jauregui, H. Cao, W. Wu, Q. Yu, Y. P Chen, *Solid State Commun.* **2011**, *151*, 1100.
[8] K. W. Clark, X. G. Zhang, I. V. Vlassiouk, Feenstra, G. He, A. P. Li, *ACS Nano* **2013**, *7*, 7956.
[9] Z. Yan, J. Lin, Z. Peng, Z. H. Sun, Y. Zhu, L. Li, Ch. Xiang, E. Lo. Samuel, C. Kittrell, J. M. Tour, *ACS Nano* **2012**, *6*, 9110.
[10] L. Gao, W. Ren, H. Xu, L. Jin, Zh. Wang, T. Ma, L. P. Ma, Zh. Zhang, Q. Fu, L. M. Peng, X. Bao, H. M. Cheng, *Nat. Commun.* **2012**, *3*, 699.
[11] H. Zhou, W. J. Yu, L. Liu, R. Cheng, Y. Chen, X. Huang, Y. Liu, Y. Wang, Y. Huang, X. Duan. *Nat. Commun.* **2013**, *4*, 2096.
[12] Y. Hao, M. S. Bharathi, L. Wang, Y. Liu, H. Chen, S. Nie, X. Wang, H. Chou, C. Tan, B. Fallahazad, H. Ramanarayan, C. W. Magnuson, E. Tutuc, B. I. Yakobson, K. F. McCarty, Y. W. Zhang, P. Kim, J. Hone, L. Colombo, R. S. Ruoff, *Science* **2013**, *342*, 720.
[13] L. Gan, Z. Luo, *ACS Nano* **2013**, *7*, 9480.
[14] J. H. Lee, E. K. Lee, W. J. Joo, Y. Jang, B. S. Kim, J. Y. Lim, S. H. Choi, S. J. Ahn, J. R. Ahn, M. H. Park, C. W. Yang, B. L. Choi, S. W. Hwang, D. Whang, *Science* **2014**, *344*, 286.
[15] Y. Ogawa, B. Hu, C. M. Orofeo, M. Tsuji, K. Ikeda, S. Mizuno, H. Hibino, H. Ago, *J. Phys. Chem. Lett.* **2012**, *3*, 219.
[16] B. Hua, H. Ago, Y. Ito, K. Kawahara, M. Tsuji, E. Magome, K. Sumitani, N. Mizuta, K. Iked, S. Mizuno, *Carbon* **2012**, *50*, 57.
[17] L. Gao, J. Guest, N. P. Guisinger, *Nano Lett.* **2010**, *10*, 3512.
[18] S. Nie, J. M. Wofford, N. C. Bartelt, O. D. Dubon, K. F. McCarty, *Phys. Rev. B* **2011**, *84*, 155425.
[19] L. Brown, E. B. Lochocki, J. Avila, Ch. J. Kim, Y. Ogawa, R. W. Havener, D. K. Kim, E. J. Monkman, D. E. Shai, H. I. Wei, M. P. Levendorf, M. Asensio, K. M. Shen, J. Park, *Nano Lett.* **2014**, *14*, 5706.
[20] J. Lahiri, Y. Lin, P. Bozkurt, I. I. Oleynik, M. Batzill, *Nat. Nanotechnol.* **2010**, *5*, 326.
[21] W. Yang, G. Chen, Zh. Shi, Ch. Ch. Liu, L. Zhang, G. Xie, M. Cheng, D. Wang, R. Yang, D. Shi, K. Watanabe, T. Taniguchi, Y. Yao, Y. Zhang, G. Zhang, *Nat. Mater.* **2013**, *12*, 792.
[22] D. W. Kim, Y. H. Kim, H. S. Jeong, H. T. Jung, *Nat. Nanotechnol.* **2012**, *7*, 29.
[23] R. W. Havener, H. Zhuang, L. Brown, R. G. Hennig, J. Park, *Nano Lett.* **2012**, *12*, 3162.
[24] K. Kim, S. Coh, L. Z. Tan, W. Regan, J. M. Yuk, E. Chatterjee, M. F. Crommie, M. L. Cohen, S. G. Louie, A. Zettl, *Phys. Rev. Lett.* **2012**, *108*, 246103.
[25] S. Coh, L. Z. Tan, S. G. Louie, M. L. Cohen, *Phys. Rev. B* **2013**, *88*, 165431.
[26] C. Lin, X. Huang, F. Ke, C. Jin, N. Tong, X. Yin, L. Gan, X. Guo, R. Zhao, W. Yang, E. Wang, Z. Hu, *Phys. Rev. B* **2014**, *89*, 085416.
[27] L. Tapasztó, P. Nemes-Incze, G. Dobrik, K. J. Yoo, Ch. Hwang, L. P Biró, *Appl. Phys. Lett.* **2012**, *100*, 053114.
[28] J. C. Koepke, J. D. Wood, D. Estrada, Z. Y. Ong, K. T. He, E. Pop, J. W. Lyding, *ACS Nano* **2013**, *7*, 75.
[29] H. Ago, Y. Ogawa, M. Tsuji, S. Mizuno, H. Hibino, *J. Phys. Chem. Lett.* **2012**, *3*, 2228
[30] Q. Yuan, L. Li, R. Au, B. I. Yakobson, F. Ding, *unpublished*.

© 2014 WILEY-VCH Verlag GmbH & Co. KGaA, Weinheim